Isochemical contact metamorphism of mafic schist, Laramie Anorthosite Complex, Wyoming: Amphibole compositions and reactions

CAROL RUSS-NABELEK*

Department of Earth and Space Sciences, State University of New York at Stony Brook, Stony Brook, New York 11794, U.S.A.

ABSTRACT

Contact metamorphism by anorthosite and syenite of the Laramie Anorthosite Complex, Wyoming, resulted in a thermal overprint of the regionally metamorphosed amphibolite-facies country rocks at approximately 3.0-kbar pressure. The resulting assemblages in the mafic schist are amp + plg + ilm ± qtz ± cpx at the lowest-grade hornblende hornfels facies, amp + plg + cpx + opx + ilm + mt ± qtz at the orthopyroxene hornfels facies boundary, and amp + plg + cpx + opx + olv + ilm + mt at the highest grade, the olivine hornfels subfacies. Clinopyroxene first appeared at temperatures of ≥670 °C, forming concomitantly with quartz from reaction of hornblende with plagioclase. Orthopyroxene first resulted from reaction of quartz with hornblende between >680 and 820 °C and above 730 °C from dehydration of hornblende where quartz was not available. Quartz appears to have persisted up to 890 °C in some bulk compositions. Olivine first appeared at 907 °C from the reaction of hornblende with plagioclase. The highest grade of contact metamorphism preserved in the mafic schist at Morton Pass was the olivine hornfels subfacies, which recorded temperatures up to 933 °C.

The dominant effect of isochemical metamorphism of these schists was the change in abundance and composition of hornblende with concomitant modal increase or decrease in the other phases. Discontinuous reactions break amphibole down to pyroxenes and plagioclase (and eventually olivine) at facies and subfacies boundaries, while continuous reactions allow for the progressive enrichment of K, Na, Al, Ti, F, and Cl as the quadrilateral amphibole component, $(Ca,Mg,Fe)_7Si_8O_{22}(OH)_2$, becomes increasingly unavailable. There appears to be a linear relationship between Al^{IV} and temperature, suggesting that systematic trends of other elements with Al^{IV} also reflect changes in temperature. Edenite $(NaAlSi_{-1}\square_{-1})$ and tschermakite $(Al_2Mg_{-1}Si_{-1})$ components best describe the enrichment of Na and Al^{IV} in amphibole with increasing temperature. There are no significant changes in the compositions of the other phases with grade. It is shown that progressive metamorphism as exemplified by the various hornfels of this study, is indicated by progressive loss of water with increasing temperature *without loss of* Cl *or* F.

Because an isochemical suite of rocks is available that spans a wide temperature range, reaction space is used to provide an effective analysis of the progress of metamorphism in the various hornfels. One effect of reaction-space modeling is the derivation of reactions specific to the formation of the facies and subfacies at Morton Pass. Although the following reactions correspond to particular samples, they exemplify the incremental changes from one grade to the next. The reaction

$$0.203amp_1 + 0.193plg = 0.155amp_3 + 1.135qtz + 0.063cpx + 0.048H_2O,$$
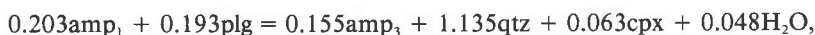
describes the initial development of clinopyroxene and was followed, at higher temperatures, by the reaction

$$0.646amp_3 + 0.101qtz + 0.030plg = 0.606amp_4 + 0.227cpx + 0.040H_2O,$$
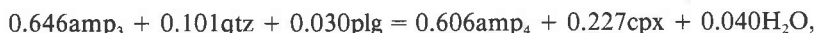
which consumed quartz rather than produced it. This reaction operated over a wide temperature range in the hornblende hornfels facies. The initial orthopyroxene-forming reaction
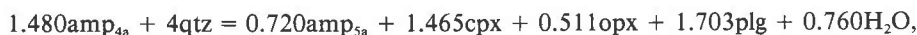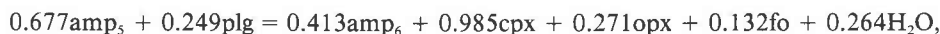
$$1.480amp_{4a} + 4qtz = 0.720amp_{5a} + 1.465cpx + 0.511opx + 1.703plg + 0.760H_2O,$$

was the major quartz-consuming reaction. After quartz reacted out, or in hornfels that were not quartz-saturated, orthopyroxene formed by a similar reaction

$$1.480amp_4 = 0.720amp_5 + 1.465cpx + 0.511opx + 0.703plg + 0.760H_2O.$$
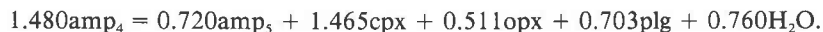
At the highest grade, olivine formed by the reaction

$$0.677amp_5 + 0.249plg = 0.413amp_6 + 0.985cpx + 0.271opx + 0.132fo + 0.264H_2O,$$

which continued within the olivine hornfels subfacies until the ultimate demise of amphibole above 940 °C.

INTRODUCTION

Previous studies (e.g., Engel and Engel, 1962a, 1962b; Harte and Graham, 1975; Laird, 1980; Laird and Albee, 1981a, 1981b; Abbott, 1982; Robinson, 1982a, 1982b; Stoddard, 1985) that have dealt with metamorphism of amphiboles in mafic systems have provided valuable information on the history and role of intensive variables during the metamorphism of specific terranes. For example, Laird (1980) described systematic amphibole compositional changes and variations in proportions of coexisting phases during low-temperature, high-pressure metamorphism of mafic schists in Vermont.

The Morton Pass area of the Laramie Anorthosite Complex, Wyoming, provides an excellent example of the effects of low-pressure, high-temperature metamorphism of mafic schists and therefore complements the study of Laird (1980). The Morton Pass area is especially suitable for evaluating mafic schist phase relations because the last metamorphism occurred in response to an isobaric thermal overprint by the anorthosite intrusion; therefore, variations in phases and their compositions primarily express changes in temperature. Because isochemical suites of the mafic rocks are available, the reactions that occurred at low pressure and medium to very high temperatures can be identified. Of particular importance with regard to these rock types is the presence of one or two pyroxenes, which, through the application of pyroxene thermometry, indicate the temperatures at which the continuous and discontinuous reactions occur.

The approach to charcterization of the Morton Pass hornfels is (1) to identify an isochemical suite of rocks spanning the temperature range of metamorphism, (2) to identify the changes in mode and mineral composition from low to high grade, and (3) to derive reactions describing the formation of facies and subfacies. Reaction space, following the procedure of Thompson et al. (1982), is used to characterize the reactions. The result of this approach is a better understanding of the amphibolite-to-granulite facies transition at low pressures in mafic rocks.

GEOLOGY OF THE CONTACT AUREOLE AT MORTON PASS

The Laramie Anorthosite Complex cores the easternmost of the three prongs of the Rocky Mountain Front Range that extend northward into southern Wyoming. The complex and its contact aureole crop out over an areal extent of more than 1000 km² in the Laramie Mountains (Fowler, 1930; Newhouse and Hagner, 1957; Klugman, 1966).

A particularly good exposure of the high-grade rocks of the contact aureole is in the Morton Pass area (Fig. 1). Archean felsic gneisses crop out in the western and central regions of this study area. The eastern edge of the gneiss sequence is in concordant contact with a supracrustal unit (Fig. 1) whose relative age is unclear but that is inferred to be younger than the gneisses (Graff et al., 1982). A metasedimentary unit of the supracrustal group is composed in the north of thin layers of impure limestone and calc-silicate that rapidly broaden southward into intercalated layers of dolomite, calc-silicate, quartzite, and pelite. A volcanoclastic unit forms a continuous 100-m-wide belt and is interlayered with the metasedimentary unit. This volcanic sequence is composed of massive and banded hornfels of mafic and ultramafic compositions.

The Archean units have been discordantly cut on the east by the Laramie Anorthosite Complex, an intrusive sequence beginning with anorthosite including gabbroic and noritic varieties and concluding the monzonite and monzosyenite (Fuhrman et al., 1983; Fuhrman, 1986; Fuhrman et al., 1988). The monzonite-monzosyenite series appears to have intruded along the contact between the anorthosite and the Archean rocks, and anorthosite is suspected to lie beneath the younger syenites. Granitoid bodies are ubiquitous in the Morton Pass area, occurring perhaps as late-stage differentiates of possibly local partial melts.

It is evident from relict textures and assemblages in the lowest-grade country rocks that before the anorthosite-syenite intrusions, the rocks of this area have been deformed at least once and regionally metamorphosed to greenschist or amphibolite facies. The mafic schists in the volcanoclastic unit at the contact were then metamorphosed by the intrusives to the hornblende hornfels and pyroxene hornfels facies. Those of the hornblende hornfels facies are interlayered with massive to finely laminated leucocratic bands. Gradations between the two types occur locally. Laminations in the massive rocks are interpreted to have formed by local shearing in the amphibolites during deformation accompanying regional metamorphism and are therefore relict features. These textures were partially to completely overprinted with increasing grade. Layering of the nonhomogeneous rocks is inter-
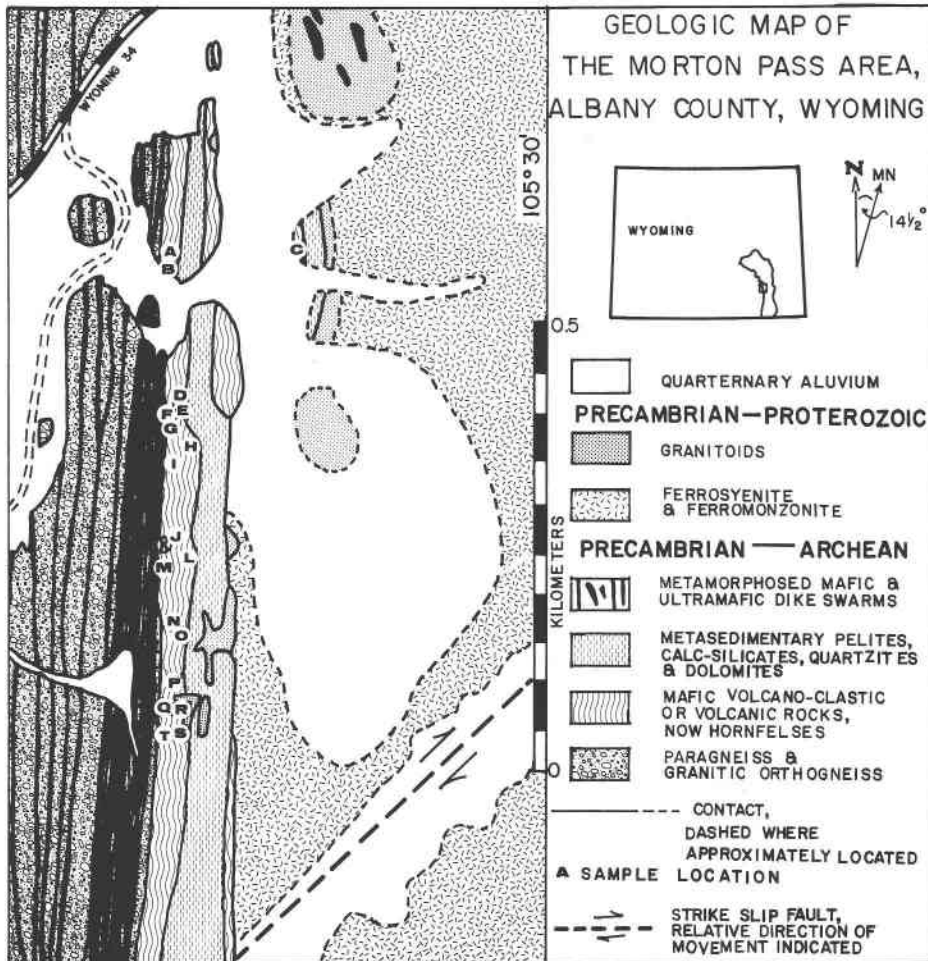
Fig. 1. Geologic map of the Morton Pass area, Albany County, Wyoming. Sample numbers referring to the letter locations are the following: A = MP11-1 and MP11-2A, B = 83-17A, C = MP12, D = MP15-4, E = MP18-1, F = 83-10, G = 83-11, H = 83-19A, I = 83-12B, J = 83-13, K = MP1-3A and MP1-3B, L = 83-14, M = 83-18, N = MP6-4, O = 83-15, P = 83-16, Q = MP3-4, R = MP3-5 and MP3-6, S = MP57-9, and T = MP57-2.

preted as a primary sedimentary feature, suggesting that these were originally volcanoclastic sediments.

The finely laminated mafic schists, the subject of this paper, occur as bands 4 cm to 5 m wide. Within these units, the degree of contact metamorphism increases to the east toward the monzosyenite.

IDENTIFICATION OF AN ISOCHEMICAL ASSEMBLAGE SERIES

The mafic schists of Morton Pass comprise a variety of bulk compositions. Two particular units were identified on stratigraphic grounds; each is effectively isochemical from low to high grade. These are referred to as "whole-rock I" and "whole-rock II" (WR I and WR II).

Whole-rock compositions were estimated by means of modal recombination. This method requires accurate modes as well as analyses of each phase. On each homogeneous thin section, 1200 point counts were made. On nonhomogeneous thin sections, the different zones were counted separately and their weighted averages combined. The modes are given in Table 1 along with the uncertainties estimated by the technique of van der Plas and Tobi (1965). Figure 2 illustrates the relative abundances of the phases in terms of volume percent. Five samples—MP11-1, 83-12B (hornblende hornfels), 83-15 (orthopyroxene hornfels), and MP3-6 and MP3-5 (olivine hornfels)—are essentially isochemical (Table 2) and are called WR I. Similarly, two samples—83-19A (hornblende hornfels) and 83-16 (pyroxene hornfels), constituting WR II—are also isochemical. Olivine hornfels sample MP3-5 was also analyzed by inductively-coupled-plasma atomic-emission spectroscopy (ICP-AES). The measured composition is nearly identical to the calculated one (Table 2). The compositions of these seven samples are comparable with oceanic tholeiites. The most compelling differences between WR I and WR II are that WR I contains quartz in at least two of the lower-grade samples and has clinopyroxene in all samples. In con-

trast, WR II has no quartz or clinopyroxene in the horn-blende hornfels facies. In accordance with field evidence for a sedimentary origin, it is suggested that prior to metamorphism, these rocks were tuffs.

PHASE ASSEMBLAGES

The major effect of contact metamorphism on Morton Pass amphibolites was the change in the abundance and composition of hornblende with concomitant changes in the proportions of other phases (Fig. 2). In general, amphibole abundance decreases along with quartz, while the proportions of plagioclase, clinopyroxene, orthopyroxene, oxides, and olivine increase. The hornfels of WR II differ from those of WR I by their greater abundance of amphibole and lack of quartz and clinopyroxene at low grades. Mineral facies in mafic schist of Morton Pass are represented by the following assemblages: hbl + plg + ilm ± cpx ± qtz (hornblende hornfels facies) and opx + cpx + hbl + plg + ilm + mag ± qtz ± olv (orthopyroxene hornfels facies). Interlayered pelitic rocks are just above the second sillimanite isograd and contain biotite + cordierite + sillimanite + K-feldspar + plg ± qtz ± spinel with rare andalusite and biotite + cordierite + garnet + K-feldspar + plg ± opx ± qtz ± spinel (Bochensky, 1982; J. A. Grant and B. R. Frost, unpublished manuscript, 1988). For the most part, there is very little chemical variation in the phases of the mafic hornfels except for amphibole, although increasing MgCa$_{-1}$ exchange component in clinopyroxene reflects increasing temperature. In fact, the "chemical evolution" of amphibole can characterize the prograde metamorphism of the mafic schist. To understand the effects of contact metamorphism on the mafic schist, it is helpful to know accurately the temperatures at which the changes took place.
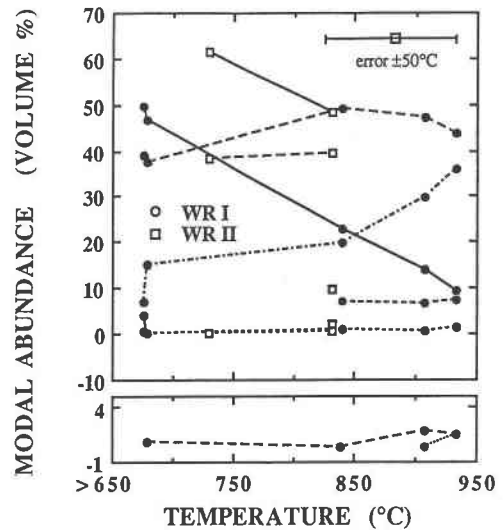

Fig. 2. Diagram showing volume percent of each phase in WR I and WR II vs. temperature estimates from pyroxene compositions. Error bars are <2% for volume and ±50 °C for temperature estimates.

ANALYTICAL TECHNIQUES

The minerals described in this study were analyzed using the former ARL EMX-SM electron microprobe at SUNY–Stony Brook. Several analyses of each phase were collected per thin section, and grains were routinely checked for zoning. Approximately 400 amphibole, 150 pyroxene, 100 plagioclase, 300 Fe-Ti oxide, and 10 olivine analyses were collected. An accelerating potential of 15 kV and a specimen current of 15 nA (referenced to brass) were used for all analyses except F and Cl, for which a specimen

TABLE 1. Modes in volume percent of phases in Morton Pass hornfels

Loc. in Fig. 1	Sample no.	Qtz	Amp	Cpx	Opx	Plg	Ilm	Mt	Olv	Apatite	Others
				Hornblende hornfels							
A	MP11-2A	7.18	57.2	—	—	35.4	0.15	—	—	tr	—
A	MP11-1	3.84	49.8	6.98	—	38.9	0.50	—	—	tr	—
J	83-13	—	47.2	13.1	—	38.9	0.11	0.80	—	tr	Calcite (tr)
I	83-12B	0.13	46.7	15.00	—	37.7	0.15	0.39	—	tr	—
E	MP18-1	tr	54.2	7.14	—	37.5	1.16	tr	—	—	—
H	83-19A	—	61.6	—	—	38.2	0.08	—	—	tr	—
B	83-17A	0.15	31.9	26.2	—	41.1	0.61	—	—	tr	—
				Orthopyroxene hornfels							
N	MP6-4	0.15	2.49	34.2	8.76	53.0	1.36	—	—	—	—
T	MP57-2	—	49.3	12.0	1.12	36.0	0.48	1.04	—	—	—
Q	MP3-4	0.16	32.6	25.5	3.69	36.9	0.96	—	—	—	—
S	MP57-9	—	31.7	20.4	4.93	40.2	0.79	1.90	—	—	Sulfide (tr)
P	83-16	—	48.3	9.90	1.95	39.6	0.30	—	—	—	—
O	83-15	—	22.8	19.8	6.90	49.2	0.90	0.41	—	tr	—
				Olivine hornfels							
R	MP3-6	—	13.9	29.9	6.46	47.1	0.49	1.88	0.25	tr	Sulfide (tr)
R	MP3-5	—	9.23	35.9	7.21	43.6	1.06	1.48	1.48	tr	Sulfide (tr)

Note: Estimated error is between 0 and 2.5% (van der Plas and Tobi, 1965). Trace amount indicated by tr.

TABLE 2. Calculated bulk compositions of WR I and WR II

| | WR I | | | | | | | | WR II | |
| | | | | | MP3-5 | | | | | |
Sample	MP11-1	83-12B	83-15	MP3-6	Calc.	Meas.*	Average	S.D.	83-19A	83-16
SiO_2	51.8	50.9	50.5	49.7	50.1	50.19	50.6	0.79	51.0	50.3
Al_2O_3	14.5	13.5	15.1	14.2	12.5	14.52	14.0	1.02	14.0	14.7
TiO_2	1.0	0.86	1.41	1.7	1.80	1.01	1.36	0.41	1.08	1.10
FeO	11.5	11.49	11.6	11.6	12.7	12.71	11.8	0.51	11.9	11.1
MnO	0.21	0.19	0.18	0.16	0.19	0.19	0.19	0.02	0.18	0.15
MgO	6.58	7.49	6.15	6.94	7.29	7.29	6.89	0.54	7.94	7.79
CaO	12.1	13.1	11.9	13.0	12.9	12.9	12.6	0.56	10.9	12.4
Na_2O	2.21	2.36	3.03	2.55	2.42	2.42	2.51	0.31	2.74	2.43
K_2O	0.05	0.12	0.10	0.17	0.11	0.11	0.11	0.04	0.18	0.13
H_2O_{calc}	2.19	nd	1.03	0.18	nd	nd	nd	nd	2.3	1.5
H_2O_{meas}**	2.54	nd	nd	nd	0.31	nd	nd	nd	nd	0.49
Total	99.95	100.01	99.97	100.02	100.01	99.61	99.99		99.92	100.1

Note: nd = not determined.
* Measured by ICP-AES, Environmental Trace Substances Research Center, University of Missouri, Columbia.
** H_2O measured after ignition of volatiles.

current of 12.5 μA was used. Unknowns were analyzed with a spot size of <10 μm or 17 μm when reintegration was necessary on exsolved phases. F and Cl were measured separately, on the same grains, with a spot size of approximately 15 μm and counting times of about 60 s. Data were reduced by the method of Bence and Albee (1968) with the correction factors of Albee and Ray (1970). The unit-cell formulae and site distributions for amphibole were obtained following the procedures of Papike et al. (1974). In this method, all Fe is initially assumed to be Fe^{2+}, and then Fe^{3+} is calculated (Table 3a). The result is the minimum estimate of Fe^{3+} that is consistent with the chemistry and stoichiometry of the amphiboles. Fe^{3+} obtained by this method is believed to be most appropriate for Morton Pass amphiboles since the various hornfels are strongly reduced and any oxy component (and consequently Fe^{3+}) in the amphiboles is therefore small (Russ, 1984). Representative analyses or averages of all phases are tabulated in Table 3.

GEOTHERMOMETRY AND GEOBAROMETRY

Contact-metamorphic temperatures have been estimated using the graphical two-pyroxene exchange thermometer of Lindsley (1983) and the analytical augite-solution-model thermometer of Davidson and Lindsley (1985). Quadrilateral components for both thermometers were projected from nonquadrilateral components using the scheme of Lindsley and Andersen (1983). The temperature estimates are listed in Table 4; error bars on both thermometers are ±50 °C. Clinopyroxenes in orthopyroxene-absent rocks are not saturated with orthopyroxene component and therefore give minimum temperatures. Graphical orthopyroxene temperatures (Lindsley, 1983)—based upon averages of all orthopyroxene data for each sample—are low, 605 to 760 °C. The graphical clinopyroxene temperatures are based on averages of clinopyroxene grains near *but not touching* orthopyroxene where orthopyroxene is present. The low temperatures calculated for the orthopyroxene grains are probably due

to the exchange of Ca for Fe and Mg between orthopyroxene and other mafic phases upon cooling.

The ranges in analytically calculated (Davidson and Lindsley, 1985) temperatures for all augites analyzed are indicated in Table 4. The wide range of temperatures observed for individual samples results mostly from variation between grains rather than from zoning in individual grains, as the grain size is usually too small for significant zoning. The maximum temperatures of the ranges appear to reflect contact-metamorphic temperatures. Any temperature values falling lower than the maximum value indicated are from grains that (1) did not equilibrate at the peak metamorphic temperature because they were not saturated with orthopyroxene component or (2) have re-equilibrated to lower-temperature compositions upon cooling.

The Davidson-Lindsley augite thermometer yields *minimum* temperatures of >670 to >770 °C for the hornblende hornfels facies, which has clinopyroxene but no orthopyroxene. Rocks from the orthopyroxene hornfels subfacies yield temperatures of about 760 to 900 °C, the lower of which appear to be reset. Temperatures of 907 and 933 °C were estimated for the olivine hornfels subfacies.

Attempts to apply the two-oxide geothermometer of Spencer and Lindsley (1981) to coexisting magnetite-ilmenite pairs were unsuccessful. The samples are strongly reduced with primary ilmenite grains having only 1 to 3 mol% Fe_2O_3. The reintegrated magnetites contain 30 to 80 mol% ulvöspinel. Such oxide-pair compositions fall in poorly calibrated regions of the thermometer near the WM buffer where the spinel and ilmenite isopleths are nearly parallel. Temperatures obtained from this method were generally low (400 to 500 °C), suggesting that oxidation-exsolution processes reset the oxide upon cooling.

A few temperature estimates were obtained from the adjacent pelites by Bochensky (1982) using two-feldspar geothermometry (Stormer, 1975) and Fe-Mg partitioning between garnet and cordierite (Thompson, 1976). Boch-

TABLE 3a. Electron-microprobe analyses and structural formulae of amphiboles from Morton Pass hornfels

Sample	WR I					WR II	
	MP11-1	83-12B	83-15	MP3-6	MP3-5	83-19A	83-16
SiO_2	47.5	47.5	44.6	43.9	41.4	47.1	47.0
Al_2O_3	7.65	7.75	9.42	11.7	11.9	7.38	7.98
FeO_T	18.4	17.3	18.7	17.0	17.0	17.3	17.0
MgO	10.6	11.2	10.3	10.3	10.3	11.6	11.8
MnO	0.26	0.27	0.18	0.14	0.17	0.26	0.19
TiO_2	1.14	1.41	2.19	2.76	2.71	1.48	1.65
CaO	11.1	11.3	11.1	11.1	10.9	11.1	11.3
Na_2O	1.18	1.20	1.97	2.53	2.44	1.05	1.37
K_2O	0.09	0.21	0.36	0.79	0.92	0.24	0.24
Total	97.9	98.1	98.7	100.3	97.8	97.5	98.5
F	0.06	nd	0.21	nd	0.35	0.08	0.14
Cl	0.03	nd	0.06	nd	0.37	0.12	0.21
			Cations per 23 oxygens				
Si	7.06	7.02	6.65	6.42	6.25	7.00	6.92
Al^{IV}	0.94	0.98	1.35	1.58	1.75	1.00	1.08
Al^{VI}	0.40	0.37	0.30	0.45	0.38	0.30	0.31
Fe^{2+}	2.29	2.14	2.33	2.08	2.15	2.14	2.10
Fe^{3+}	0.0	0.0	0.0	0.0	0.0	0.02	0.0
Mg	2.35	2.47	2.29	2.24	2.31	2.57	2.59
Mn	0.03	0.03	0.02	0.02	0.02	0.03	0.02
Ti	0.13	0.16	0.25	0.30	0.31	0.17	0.18
Ca	1.77	1.79	1.77	1.74	1.76	1.77	1.78
Na(M4)	0.03	0.04	0.04	0.17	0.07	0.0	0.02
Na(A)	0.31	0.30	0.53	0.55	0.65	0.30	0.38
K	0.02	0.04	0.07	0.15	0.18	0.05	0.04
A site	0.34	0.34	0.60	0.70	0.82	0.35	0.42
F	0.03	nd	0.10	nd	0.17	0.04	0.05
Cl	0.01	nd	0.01	nd	0.10	0.03	0.05
OH*	1.96	nd	1.89	nd	1.73	1.93	1.90
Mg/Fe	1.03	1.15	0.98	1.08	1.07	1.20	1.23

Note: nd = not determined.
* OH calculated as $2 - (F + Cl)$.

ensky's two-feldspar temperature range (655 to 708 °C) obtained for his sample MP-1 is about 100 °C lower than the 812 °C temperature estimated for the nearby orthopyroxene hornfels MP12. The estimate of 715 ± 60 °C for his sample MP-705 using the garnet-cordierite geo-thermometer also yields a value lower than temperature estimates from orthopyroxene hornfels of that area. This lower temperature may be the result of poor calibration of this geothermometer and/or re-equilibration of Fe and Mg between garnet and cordierite upon cooling, an in-

TABLE 3b. Average electron-microprobe analyses and structural formulae of pyroxenes from Morton Pass hornfels

Sample	WR I								WR II	
	MP11-1	83-12B	83-15		MP3-6		MP3-5		83-16	
	cpx	cpx	cpx	opx	cpx	opx	cpx	opx	cpx	opx
SiO_2	51.7	52.9	52.6	51.2	51.9	50.8	52.0	51.5	53.3	51.5
Al_2O_3	1.03	0.68	1.29	0.68	1.37	1.30	1.66	1.02	1.11	0.98
FeO	13.4	12.3	14.5	32.8	12.4	29.3	13.2	29.1	12.1	29.7
MgO	10.7	11.6	11.3	14.9	12.7	17.5	12.0	17.2	11.9	16.3
MnO	0.43	0.33	0.3	0.70	0.24	0.5	0.25	0.55	0.25	0.68
TiO_2	0.14	0.03	0.05	0.06	0.25	0.25	0.08	0.07	0.01	0.03
CaO	21.9	22.8	20.7	0.82	20.9	0.88	20.8	0.73	21.5	0.62
Na_2O	0.19	0.09	0.23	0.00	0.38	0.00	0.14	0.00		
Total	99.4	100.7	101.0	101.1	100.1	100.5	100.1	100.1	100.3	99.9
				Cations per 6 oxygens						
Si	1.91	1.99	1.98	1.98	1.95	1.95	1.97	1.98	2.00	1.99
Al	0.05	0.03	0.06	0.03	0.06	0.06	0.07	0.06	0.05	0.05
Fe^{2+}	0.43	0.39	0.46	1.06	0.34	0.94	0.42	0.94	0.38	0.96
Fe^{3+}	0.00	0.00	0.00	0.00	0.05	0.04	0.00	0.00	0.00	0.00
Mg	0.61	0.65	0.63	0.86	0.71	1.00	0.67	0.99	0.67	0.94
Mn	0.01	0.01	0.01	0.02	0.01	0.02	0.01	0.02	0.01	0.02
Ti	0.00	0.00	0.00	0.00	0.01	0.00	0.00	0.00	0.00	0.00
Ca	0.90	0.92	0.84	0.03	0.84	0.04	0.84	0.03	0.86	0.03
Na	0.01	0.01	0.02	0.00	0.03	0.00	0.01	0.00	0.01	0.00

TABLE 3c.   Average electron-microprobe analyses and structural formulae of plagioclase, ilmenite, magnetite, and olivine in Morton

| | Plagioclase | | | | | | |
| | WR I | | | | | WR II | |
	MP11-1	83-12B	83-15	MP3-6	MP3-5	83-19A	83-16
SiO_2	53.4	55.4	55.7	54.5	55.8	57.4	54.0
Al_2O_3	29.5	28.6	28.7	28.5	28.1	27.40	29.6
FeO	0.23	0.20	0.15	0.29	0.21	0.19	0.15
MgO	—	—	—	—	—	—	—
MnO	—	—	—	—	—	—	—
TiO_2	—	—	—	—	—	—	—
CaO	12.6	11.4	10.9	11.1	10.4	10.5	11.9
Na_2O	4.47	5.25	5.75	4.94	5.61	6.18	4.85
K_2O	0.01	0.05	0.03	0.12	0.06	0.06	0.01
Total	99.4	100.94	101.2	99.40	100.1	101.3	100.6
Cations per 8 oxygens							
Si	2.41	2.48	2.48	2.47	2.51	2.55	2.43
Al	1.57	1.51	1.51	1.52	1.49	1.43	1.57
Fe	0.01	0.01	0.01	0.01	0.01	0.01	0.01
Fe^{3+}	—	—	—	—	—	—	—
Mg	—	—	—	—	—	—	—
Mn	—	—	—	—	—	—	—
Ti	—	—	—	—	—	—	—
Ca	0.61	0.55	0.52	0.54	0.50	0.48	0.58
Na	0.39	0.46	0.50	0.43	0.49	0.53	0.42
K	0.00	0.00	0.00	0.01	0.00	0.00	0.00
An	61	54	51	55	50	47	58
Ilm							
Hem							
Usp							
Mt							
Fa							

* Fe^{3+} in oxides was estimated by charge balance. Mineral end-member compositions given in mole percent.

trinsic problem with this geothermometer (Essene, 1982). Pressure was estimated at approximately 3 kbar by Fuhrman (1986), Fuhrman et al. (1988), and Grant and Frost (unpublished manuscript, 1988).

The temperature estimates at Morton Pass are >676 to >776 °C for the hornblende hornfels and 760 to 933 °C for the pyroxene hornfels. In SiO_2-saturated rocks, clinopyroxene formed at temperatures of >676 °C, and orthopyroxene formed between 680 and 827 °C. No quartz was observed in rocks recording temperatures above 890 °C. In SiO_2-undersaturated rocks, the assemblage hbl + plg + ilm persisted to >730 °C, clinopyroxene and orthopyroxene appeared between 760 and 830 °C, and olivine occurs in rocks metamorphosed at about 905 °C and above. The isotherms inferred from contact metamorphism are shown in Figure 3. The fluctuations in the isotherms at the highest grade may reflect the uncertainties in temperature estimates; notwithstanding, they also suggest that igneous rock is present directly under the supracrustals.

THE CHEMICAL EVOLUTION OF AMPHIBOLE

Samples from WR I and WR II are representative of the mafic hornfels in Morton Pass, and their phase compositions relative to temperature are used to develop a quantitative model to characterize prograde metamor-

phism. Although there is variation in the proportions among the phases with grade (Fig. 2), there is little compositional variation in phases other than amphibole. This suggests that there is a strong relationship between the modal abundance of the other phases and amphibole composition. The chemographic relations of the mafic phases plotted on the quadrilateral (QUAD) plane are shown in Figures 4A and 4B. Numbers 1 through 5 (Fig. 4A) and 1 and 2 (Fig. 4B) indicate the prograde sequence. There is little change in the relative proportions of QUAD components in the amphiboles with increasing metamorphism although a slight increase in Mg/Fe is indicated. However, there is progressive enrichment of the non-QUAD components (Fig. 5). The increase of non-QUAD components can be explained by the consumption of QUAD components during reactions that form other phases. The composition of the remaining amphiboles evolves by continuous reactions, resulting in amphiboles enriched in non-QUAD components.

The increase of total Al with increasing grade is particularly intriguing. Al^{VI}, an empirical indicator of pressure (Leake, 1965; Hynes, 1982; Hammerstrom and Zen, 1986) has no systematic variation (Fig. 5A) but Al^{IV} clearly increases with grade. The correlation coefficients in Table 5 show a measure of the linear relationship between any two of the variables listed. Both Table 5 and Figure 6

Pass hornfels

	Oxides*							Olivine	
	WR I						WR II	WR I	
MP11-1	83-12B		83-15		MP3-5		83-16		
Ilm	Ilm	Mt	Ilm	Mt	Ilm	Mt	Ilm	MP3-6	MP3-5
0.22	0.14	0.48	0.17	0.48	0.38	0.96	0.11	32.2	34.2
0.25	0.19	1.53	0.62	1.99	0.18	1.12	50.5	0.0	0.01
44.1	45.8	87.59	46.5	74.0	46.1	67.9	47.1	51.2	49.6
0.0	0.11	0.0	0.27	0.03	0.03	0.11	0.08	16.0	15.5
4.0	1.9	0.17	0.78	0.44	0.54	0.45	1.06	0.63	0.56
48.7	53.3	2.90	51.5	16.1	51.5	24.7	0.49	—	—
—	—	—	—	—	—	—	—	0.0	0.11
—	—	—	—	—	—	—	—	—	—
97.3	101.4	92.66	99.9	93.1	98.8	95.2	98.9	100.0	100.0
			Cations per 3 or 4 oxygens					Cations per 4 oxygens	
0.01	0.00	0.02	0.00	0.02	0.01	0.04	0.00	0.99	1.02
0.01	0.01	0.07	0.02	0.09	0.01	0.05	0.00	0.00	0.00
0.87	1.00	1.10	0.95	1.47	1.00	1.73	0.94	1.30	1.24
0.09	0.00	1.73	0.03	0.93	0.00	0.45	0.06	—	—
0.00	0.00	0.00	0.01	0.00	0.00	0.01	0.00	0.72	0.69
0.09	0.04	0.01	0.02	0.01	0.01	0.01	0.02	0.02	0.01
0.95	1.00	0.08	0.97	0.47	1.00	0.71	0.97	—	—
—	—	—	—	—	—	—	—	0.00	0.00
—	—	—	—	—	—	—	—	—	—
—	—	—	—	—	—	—	—	—	—
95.2	100.3		98.7		100.0		97.00		
4.8	−0.28		1.31		−0.02		3.00		
		8.30		47.7		74.4			
		91.7		52.3		25.6			
								64	64

suggest that, at least for WR I and WR II samples, the concentration of Al^{IV} is dependent on temperature. In fact, it appears that for assemblages that include hbl + plg as the only aluminous phases, Al^{IV} in amphibole may be used as a thermometer (Russ, 1984; Russ and Lindsley, 1984; Nabelek and Lindsley, 1985; Russ-Nabelek and Lindsley, work in progress). Thus, variation in amphibole components with respect to Al^{IV} are relevant to changes in temperature. In Figures 5A through 5D, the enclosed areas indicate values for 282 analyses of amphibole from Morton Pass and HbH (hornblende hornfels), OpH (orthopyroxene hornfels), and OlH (olivine hornfels) mark the different facies or subfacies. The overlap of the HbH, OpH, and OlH fields is an indirect result of bulk-composition differences between amphiboles in all the mafic schists plotted and reflects amphibole composition in rocks with quartz where orthopyroxene may have formed relatively early. The line of slope 1.0 in Figure 5A corresponds to a Tschermak substitution vector ($Al^{VI}Al^{IV}Mg_{-1}Si_{-1}$). A pure Ti-Tschermak substitution from tremolite (Fig. 5B) requires a 1:2 ratio of Ti to Al^{IV}. The nearly parallel path with slope ½ of the Ti-Tschermak vector to the Ti abundance in amphibole shows that the total amount of Ti may be described by this vector but not Al^{IV}. Al^{VI}, Fe^{3+}, and Ti^{4+} (Fig. 5C) are preferentially ordered into the amphibole M2 site, causing site
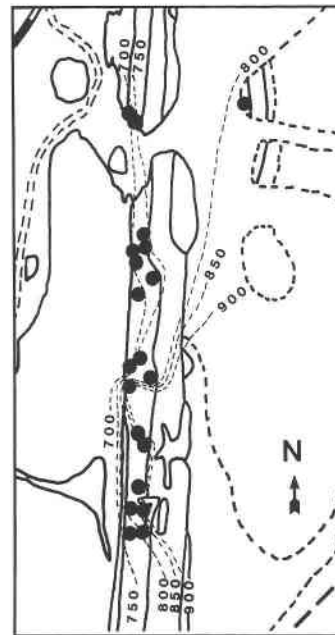

Fig. 3. Map of isotherms in mafic schists at Morton Pass. Solid circles indicate sample locations. Fluctuations in the isotherms suggest that igneous rocks may be present beneath parts of the supracrustal unit.
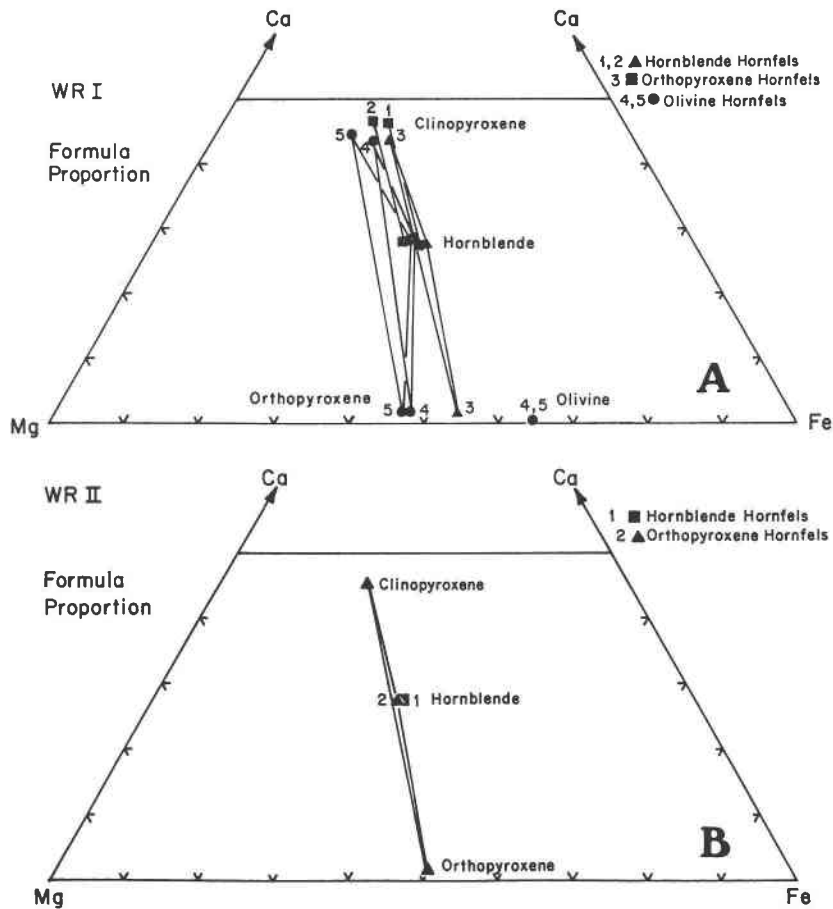
Fig. 4. (A) Chemographic relations of mafic phases in WR I plotted on QUAD. Numbers 1 through 5 indicate the prograde sequence. (B) Chemographic relations of mafic phases in WR II, plotted on QUAD. Numbers 1 and 2 indicate the prograde sequence.

charge imbalances of $+1$ or $+2$. The excess charge is counterbalanced by Al^{3+} substitution for Si in the tetrahedral site as well as Na for Ca in the M4 site (Cameron and Papike, 1979). Thus, a positive trend in $Fe^{3+} + 2Ti + Al^{VI}$ suggests that M2-site occupancy of these components is indirectly related to temperature increases. For M2-site occupancy of pure Fe^{3+}, Ti^{4+}, Al^{3+}, or any combination thereof, a 1:1 or 1:2 correlation with Al^{IV} is required, giving a ferri-Tschermak, Ti-Tschermak, or Tschermak composition. From Figure 5C it is obvious that a combination of these substitutions is responsible for M2-site occupancy. The trend in A-site occupancy with increasing grade lies along a line with slope of about 0.5 and Al^{IV} intercept of 0.5, intersecting the pargasitic trend only at high grade. Similar to the filling of the M2 site, A-site occupancy must also counterbalance charges in the tetrahedral site. Because the pargasite compositional trend is the sum of 1 Tschermak and 1 edenite substitution ($NaAlSi_{-1}\square_{-1}$), the unique A-site compositional trend for Morton Pass amphiboles is due to a ratio other than 1:1 for these substitutions. Indeed, it is suggested that A-site occupancy with Al^{IV} edenite substitu-

tions dominate over the Tschermak substitutions in order to maintain the required charge balance. The perfect correlation (Table 5) of ED (edenite exchange component) with Al^{IV} indicates that edenite is the dominant component for Al^{IV} enrichment and that plagioclase exchange ($NaSiCa_{-1}Al_{-1}$) is the least prevalent.

K, F, and Cl appear to be retained in the residual amphibole. For example, K content is inversely proportional to the volume percent of amphibole in WR I rocks (Fig. 7A). Regression of the curve (Fig. 7A) gives the relation K (in formula proportion units) = $1.75 \pm 0.11 \div$ vol% amphibole. F and Cl are also progressively enriched in amphiboles with decreasing amphibole abundance (Fig. 7B), giving the relations F (in formula proportion units) = $1.66 \pm 0.17 \div$ vol% amphibole and Cl (in formula proportion units) = $0.82 \pm 0.17 \div$ vol% amphibole. Amphiboles from WR II have less F but the same amounts of Cl as equivalent amphiboles from WR I. The inverse relationship with volume percent amphibole (not shown) is the same, however, suggesting that amphibole breakdown is almost entirely a dehydration process.

With rising temperature and amphibole breakdown,

TABLE 4. Temperatures of metamorphism of Morton Pass hornfels

Loc. in Fig. 1	Sample	Graphical thermometer*		Analytical thermometer**
		Cpx	Opx	Aug (T range)†
Hornblende hornfels				
A	MP11-1	>657		>676 (>645 to >676)
B	83-17A	>690		>759 (>640 to >759)
D	MP15-4	>690		>734 (>661 to >734)
F	83-10	>630		>741 (>621 to >741)
G	83-11	>605		>726
I	83-12B	>620		>679 (>623 to >679)
H	83-19A††	>670		>729 (>592 to >729)
J	83-13	>500‡		>776
E	MP18-1	>650		>740 (>663 to >740)
K	MP1-3A	>620		>676
Orthopyroxene hornfels				
M	83-18	830 to 950	610	903 (695 to 903)
O	83-15	805	605	839 (793 to 839)
L	83-14	760	610	760‡ (711 to 760)
N	MP6-4	715	640	889 (649 to 889)
Q	MP3-4	720	710	827 (743 to 827)
P	83-16	780	650	831 (769 to 831)
T	MP57-2	715	610	773‡ (687 to 773)
S	MP57-9	755	640	872 (714 to 872)
Olivine hornfels				
R	MP3-6	850	710	907 (816 to 907)
R	MP3-5	870	760	933 (813 to 933)
	From Bochensky (1982):		Feld‡‡	Cord-Gar§
	MP-1		655 to 708	
	MP-203			707 (±60)
	MP-705			715 (±60)

* Graphical temperatures based on the thermometer of Lindsley (1983). The temperatures are based on average pyroxene compositions assuming 3-kbar pressure. *Minimum temperatures* are from rocks with no orthopyroxene. Uncertainties are ±50 °C.
** Temperature estimates based on solution model "A" of Davidson and Lindsley (1985) assuming 3-kbar pressure. *Minimum temperatures* are from rocks without orthopyroxene. Uncertainties are ±50 °C.
† Range of temperatures calculated for all grains analyzed.
†† Sample 83-19A does not have clinopyroxene. Temperatures were estimated from clinopyroxene grains in the reaction rim that divides the mafic layer from a calc-silicate layer.
‡ Probably reset.
‡‡ Temperatures from two-feldspar geothermometer (Stormer, 1975).
§ Cordierite-garnet temperatures after Thompson (1976).

TABLE 5. Linear correlation of amphibole components and temperature for WR I and WR II

	Al^{IV}	T	PL	ED	TK
Al^{IV}	1.00				
T	0.92	1.00			
PL	0.88	0.77	1.00		
ED	0.98	0.95	0.80	1.00	
TK	0.97	0.93	0.94	0.94	1.00

PL = $NaSiCa_{-1}Al_{-1}$
ED = $NaAlSi_{-1}$
TK = $Al^{VI}Al^{IV}Mg_{-1}Si_{-1}$

progress of such reactions along a P, T, f_{H_2O} path can be calculated and is particularly useful in quantifying prograde metamorphism when an isochemical series of samples is available for which temperatures are known.

To visualize the progress of the net-transfer reactions that transform an initial assemblage into the final assemblage at Morton Pass, reaction space, as developed by Thompson et al. (1982), is utilized. The subassemblage amp + plg ± pyx ± (olv or qtz) is compositionally defined by the oxides SiO_2, Al_2O_3, FeO, Fe_2O_3, MgO, MnO, TiO_2, CaO, Na_2O, K_2O, and H_2O, which may be condensed into the subspace Na_2O, CaO, MgO, Al_2O_3, SiO_2, and H_2O (NCMASH) (Thompson et al., 1982). Because the system is open and H_2O is continuously lost, water is treated as a separate phase denoted "env." Nine possible exchange components (Table 6) operate within and between the additive components amphibole, plagioclase, pyroxene, and olivine, but only TK, ED, PL, and $MgCa_{-1}$ (see above) are considered here to be significant. The phases among which continuous exchange reactions may

TABLE 6. Reaction components, phases, and notation for the mafic schist subassemblage

Component		Mineral phase
Additive component		
$NaAlSi_3O_8$	(ab)	plg
$Ca_2Mg_5Si_8O_{22}(OH)_2$	(tr)	amp
$CaMgSi_2O_6$	(di)*	pyx
SiO_2	(qz)	qtz
Mg_2SiO_4	(fo)	olv
H_2O	(env)	H_2O
Exchange component		
$Al_2Mg_{-1}Si_{-1}$	(TK)	amp, pyx**
$NaAlSi_{-1}$	(ED)	amp, pyx
$NaSiCa_{-1}Al_{-1}$	(PL)	amp, plg, pyx
$MgCa_{-1}$	$(MgCa_{-1})$	amp, pyx, olv
Other possible exchange components		
$FeAl_{-1}$		amp, pyx
$FeMg_{-1}$		amp, pyx, olv
$FeTiFe_{-2}$	$(TiFe_{-1})$	amp
KNa_{-1}		amp, plg
$MnFe_{-1}$		amp, pyx, olv

Note: The convention *lowercase* letters for *additive components* and *UPPERCASE* for *exchange components* (as shown, except for $MgCa_{-1}$) is used throughout the text.
* Additive component di is sufficient to describe both clinopyroxene and orthopyroxene because di + $MgCa_{-1}$ = enstatite; hence they are not linearly independent.
** E.g., $Al_2Mg_{-1}Si_{-1}$ in amphibole = $Al_2Mg_{-1}Si_{-1}$ in pyroxene.

continuous reactions enrich the remaining amphiboles in non-QUAD components as QUAD amphibole component becomes unavailable. These changes are best shown through the substitution operators Tschermak, edenite, KNa_{-1}, $ClOH_{-1}$, and FOH_{-1}, respectively (Thompson, 1982; Thompson et al., 1982). The prograde enrichment trends of edenite, Tschermak, and KNa_{-1} components for the hornblende hornfels facies and the orthopyroxene and olivine hornfels subfacies of the pyroxene hornfels facies are shown in Figure 8.

REACTION SPACE

Simple exchange reactions and net-transfer reactions, which have both additive components (phases) and exchange components, can describe modal and compositional changes of phases from one facies to another. The
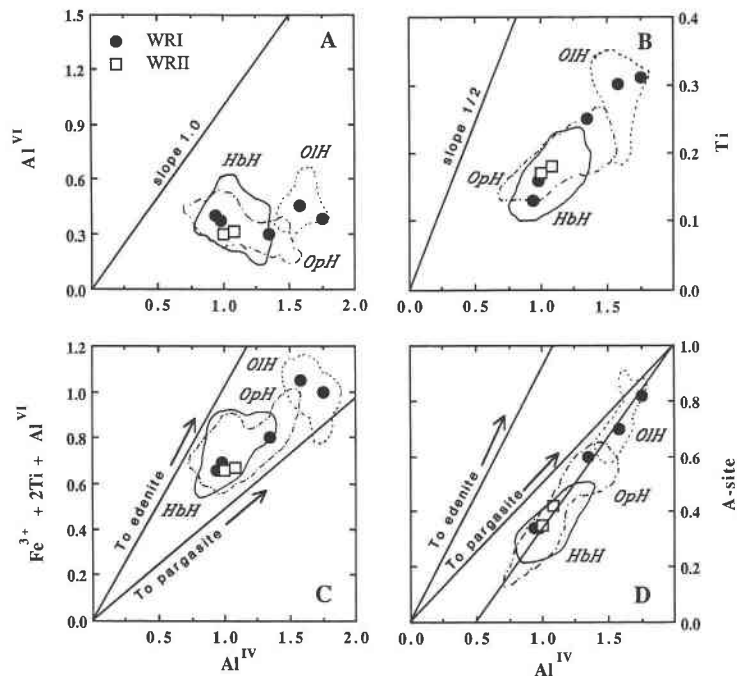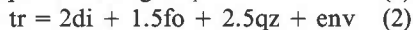
Fig. 5. Variations of site occupancies with Al^{IV}. (**A**) Plot of Al^{VI} vs. Al^{IV} shows very little systematic variation. The line of slope 1 corresponds to pure tschermakitic substitution from tremolite at the origin. The enclosed areas represent amphiboles from all mafic schist analyzed at Morton Pass. HbH = hornblende hornfels facies, OpH = orthopyroxene hornfels subfacies, OlH = olivine hornfels subfacies. Circles are *averaged* analyses from WR I; squares are *averaged* analyses from WR II. (**B**) Plot of Ti vs. Al^{IV} shows a positive enrichment trend for Ti in amphibole. Ratio of 1 Ti to 2 Al^{IV} is the Ti-Tschermak substitution. (**C**) Plot of $Fe^{3+} + 2(Ti) + Al^{VI}$ vs. Al^{IV} illustrates M2-site substitution in amphibole with increasing grade. Ferri-Tschermak and Tschermak substitutions operate along a line of 1:1. Ti-Tschermak operates along a line of 1:2. (**D**) Plot of A-site occupancy vs. Al^{IV}; A-site substitution is described by the line A-site $= 0.5Al^{IV} - 0.25$.

occur are indicated to the right in Table 6. All other exchange components possible in the 12-oxide compositional space may be accessed from the condensed space.

Transformation of the NCMASH oxide components into the phase components (tr, ab, di, qz, fo, and env) and exchange components (TK, ED, PL, and $MgCa_{-1}$) yields a set of four independent net-transfer reactions:

$$fo + qz = di + MgCa_{-1} \qquad (1)$$
$$tr = 2di + 1.5fo + 2.5qz + env \qquad (2)$$
$$ab = 4qz + ED \qquad (3)$$
$$di + qz + PL + TK = ab. \qquad (4)$$

These reactions are sufficient to describe the modal and compositional variations in phases in the defined 12-oxide compositional space of the Morton Pass hornfels. Note that Equation 1 becomes more familiar if $MgCa_{-1}$ is combined with di to become fo + qz = enstatite. Particular linear combinations of Reactions 1 to 4 can eliminate one or more select phases and result in reactions that have the subassemblages observed at Morton Pass. Because of the constraints of working in three- rather than four-dimensional space, two polygons have been devised to show reaction progress in the quartz-bearing and quartz-absent
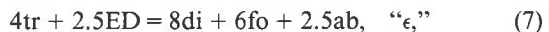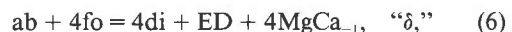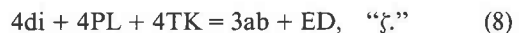
rocks. The reactions

$$tr = 3.5di + qz + 1.5MgCa_{-1}, \quad \text{“}\alpha\text{,”} \qquad (5)$$

$$ab = 4qz + ED, \quad \text{“}\beta\text{,”} \qquad (3)$$

and

$$di + qz + PL + TK = ab, \quad \text{“}\gamma\text{”} \qquad (4)$$
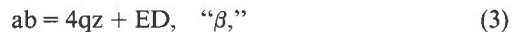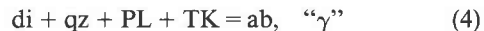
are the axes of a polygonal coordinate system determined for quartz-bearing rocks (Fig. 9). Equation 5 is a simple combination of Reactions 1 and 2 that eliminates olivine. By making linear combinations of Reaction 3 with Reactions 1, 2, and 4 to eliminate quartz, the following reactions for quartz-absent rocks are determined:

$$ab + 4fo = 4di + ED + 4MgCa_{-1}, \quad \text{“}\delta\text{,”} \qquad (6)$$

$$4tr + 2.5ED = 8di + 6fo + 2.5ab, \quad \text{“}\epsilon\text{,”} \qquad (7)$$

and

$$4di + 4PL + 4TK = 3ab + ED, \quad \text{“}\zeta\text{.”} \qquad (8)$$

Both reaction spaces, the first necessitating the presence of quartz and the second allowing for the formation of
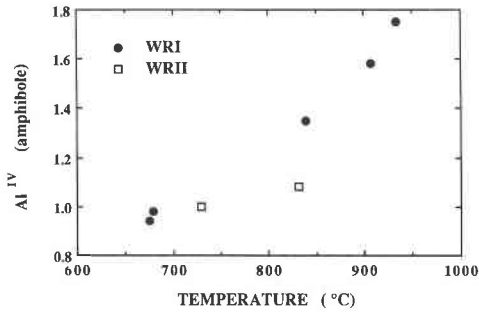
Fig. 6. Plot of Al^{IV} vs. temperature, from WR I and WR II pyroxene temperature estimates, suggests that Al^{IV} in amphibole is a function of temperature.

Fig. 8. Prograde enrichment trend of KNa_{-1}, Tschermak, and edenite components in WR I amphiboles. The hornblende hornfels facies is unlabeled; orthopyroxene and olivine hornfels subfacies are indicated. Temperatures derived from clinopyroxene thermometry are also shown.

olivine, are therefore related by Reaction 3. Linear combinations of these reactions are vectors. From inspection of both sets of reactions, one can identify particular combinations of reactions that occurred at Morton Pass. As a reference point, unpublished experimental results on the olivine hornfels MP3-5 recrystallized at 600 °C and 3 kbar were used. The experimental amphibole and plagioclase compositions make an excellent reference point for the models, because the rock under these pressure and temperature conditions must be similar to the precursor of the contact-metamorphic assemblages of WR I. The composition and estimated mode of the reference-point amphibolite are listed in Table 7.

The bounding planes of the reaction-space polyhedra (Figs. 9 and 10) indicate (1) the limits of exchange-component capacity and (2) the limit of availability of a phase for reaction. Exchange-component limits are the minimum and maximum operations of the exchange components in the phases (indicated in Table 6) in which they occur, for example [TK−] and [TK+] indicate the minimum and maximum amount of $Al^{VI}Al^{IV}Mg_{-1}Si_{-1}$ in additive components tr and di. The reaction limits of additive components form planes where phases disappear. Phases not present in the original assemblage are formed as metamorphism proceeds but do not form bounding
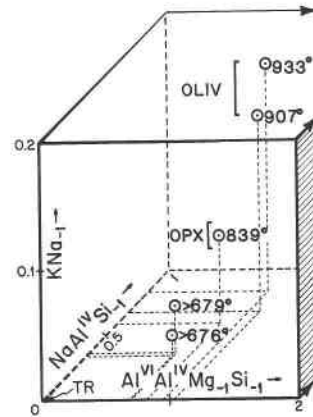
planes (e.g., di + fo) unless they react out of the assemblage. The modal amount of each phase may be represented by the number of oxygen units in its additive component (ad) (Thompson et al.). Δn_{ad} (Table 7) is the change in the number of oxygen units of each of the additive components as a result of reactions α, β, and γ or δ, ϵ, and ζ. The total distribution of the exchange components and additive components between the reaction vectors of each polygon is listed in Table 7. The poles to the bounding planes of the polyhedra are also vectors; if shown, they would intersect at the origin and have magnitude and direction specified by the equations in Table 7. Not all exchange or additive components form bounding planes because the limits of exchange of the former can never be reached or the latter will never be totally consumed. Because in some cases, the mineral composition is known better than the mode. n_{ex} (Table 7) is replaced by the quantity $(X_{ex}n_{ad})/e$, where e is the number of oxygen equivalents per mole of additive component. To ob-
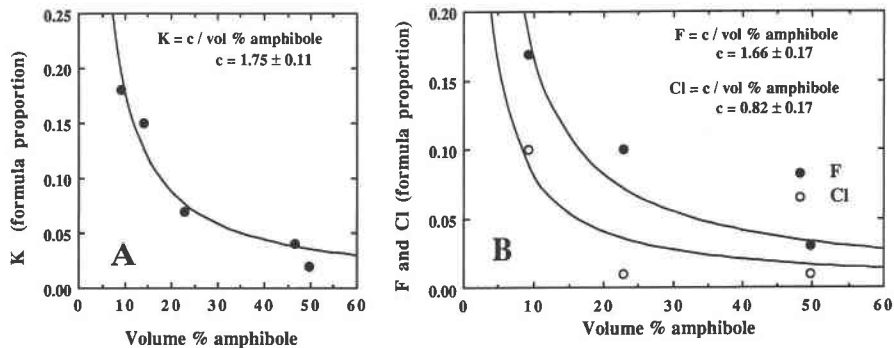

Fig. 7. (A) Volume percent of amphibole vs. K (in formula proportion units) for WR I. (B) Volume percent of amphibole vs. F and Cl (in formula proportion units) in WR I.
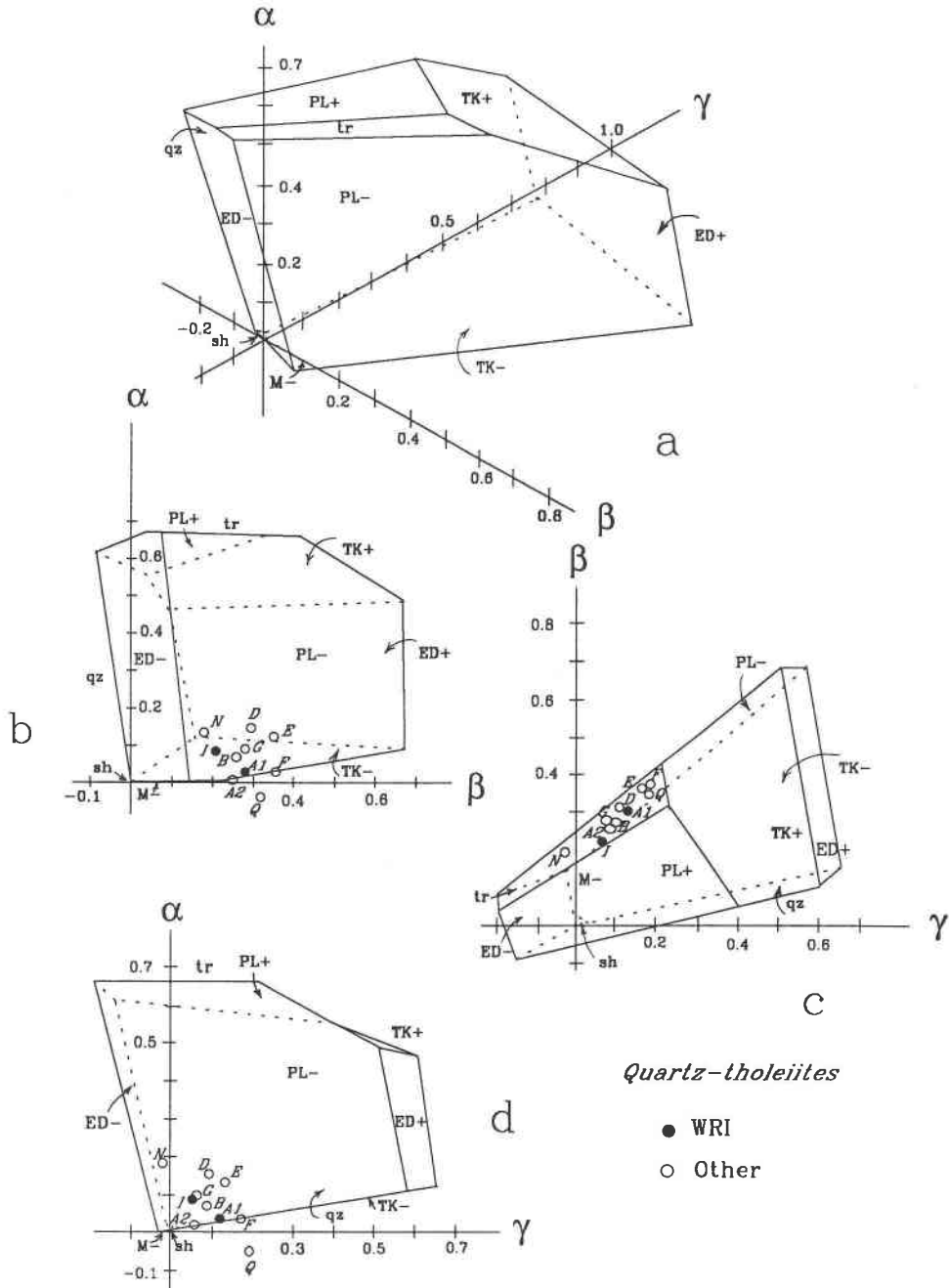
Fig. 9. (a) Quartz tholeiite reaction-space polygon corresponding to olivine hornfels MP3-5 of olivine tholeiite composition with 5 vol% quartz. The coordinate axes α, β, and γ indicate advancement along (net-transfer) Reactions 5, 3, and 4. The faces of the polygon are bounding planes, indicating the point of elimination of additive components or the limits of exchange capacity. MgCa$_{-1}$ is abbreviated as M$-$. (b), (c), and (d) are orthographic views. Letters refer to particular samples and correspond to the sample numbers and locations in Fig. 1 and temperatures in Table 4.

tain mass-balance equations for each exchange component, the quantity $(X_{ex}n_{ad}/e)$ and the equations of Table 7 were substituted into the equation of Ferry (1984)

$$\sum_j X^0_{i,j}n^0_j + \sum_k \nu_{i,k}\xi_k = \sum_j X^f_{i,j}\left(n^0_j + \sum_k \nu_{j,k}\xi_k\right), \quad (9)$$

where i = exchange component i, j = additive component j, k = a specific net-transfer reaction (α, β, γ, δ, ϵ, or ζ), ξ = progress of Reaction α, β, γ, δ, ϵ, or ζ, $X_{i,j}$ = mole fraction of component i in phase j, $\nu_{i,j}$ = the stoichiometric coefficient of exchange component i, in Reaction α, β, γ, δ, ϵ, or ζ, n_j = the number of moles of phase j, and the

TABLE 7. Distribution of the additive and phase components among Reactions α, β, γ, δ, ϵ, and ζ

Plane		Reference-point amphibolite
	Quartz tholeiite model applied to rocks with tr + ab + qz ± di	
tr	$\Delta n_{tr} = n_{tr} - n_{tr}^0 = -\Delta\alpha^*$	$2n_{tr}^0 = 0.655^{**}$
ab	$\Delta n_{ab} = n_{ab} - n_{ab}^0 = \Delta\beta + \Delta\gamma$	$n_{ab}^0 = 0.340^{**}$
di	$\Delta n_{di} = n_{di} - n_{di}^0 = 0.875\Delta\alpha - 0.75\Delta\gamma$	$3n_{di}^0 = 0^{**}$
qz	$\Delta n_{qz} = n_{qz} - n_{qz}^0 = 0.083\Delta\alpha - \Delta\beta - 0.25\Delta\gamma$	$n_{qz}^0 = 0^{**}$
TK	$n_{TK} - n_{TK}^0 = -0.125\Delta\gamma$	$X_{TK}^{0,tr} = 0.677$
ED	$n_{ED} - n_{ED}^0 = -0.125\Delta\beta$	$X_{ED}^{0,tr} = 0.196$
PL	$n_{PL} - n_{PL}^0 = -0.125\Delta\gamma$	$X_{PL}^{0,tr} = 0.137$ $X_{PL}^{0,ab} = 0.502$
MgCa$_{-1}$	$n_{MgCa_{-1}} - n_{MgCa_{-1}}^0 = 0.063\Delta\alpha$	$X_{MgCa_{-1}}^{0,tr} = 0.195$
sh	$0 = 0.063\Delta\alpha + 0.125\Delta\beta$	
	Olivine tholeiite model applied to rocks with tr + ab + di ± fo	
tr	$\Delta n_{tr} = n_{tr} - n_{tr}^0 = -\Delta\epsilon$	$n_{tr}^0 = 0.657†$
ab	$\Delta n_{ab} = n_{ab} - n_{ab}^0 = 0.333\Delta\delta + 0.208\Delta\epsilon + \Delta\zeta$	$n_{ab}^0 = 0.343†$
di	$\Delta n_{di} = n_{di} - n_{di}^0 = \Delta\delta + 0.5\Delta\epsilon - \Delta\zeta$	$n_{di}^0 = 0†$
fo	$\Delta n_{fo} = n_{fo} - n_{fo}^0 = 0.667\Delta\delta + 0.25\Delta\epsilon$	$n_{fo}^0 = 0†$
TK	$n_{TK} - n_{TK}^0 = -0.167\Delta\zeta$	$X_{TK}^{0,tr} = 0.677$
ED	$n_{ED} - n_{ED}^0 = 0.042\Delta\delta - 0.026\Delta\epsilon + 0.042\Delta\zeta$	$X_{ED}^{0,tr} = 0.196$
PL	$n_{PL} - n_{PL}^0 = -0.167\Delta\zeta$	$X_{PL}^{0,tr} = 0.137$ $X_{PL}^{0,ab} = 0.502$
MgCa$_{-1}$	$n_{MgCa_{-1}} - n_{MgCa_{-1}}^0 = 0.167\Delta\delta$	$X_{MgCa_{-1}}^0 = 0.195$
sh	$0 = 0.042\Delta\delta - 0.026\Delta\epsilon + 0.042\Delta\zeta$	

Note: For definition of variables, see text.
 * E.g., (final mode of amphibole) − (initial mode of amphibole) is equivalent to 1 negative unit of advancement along α.
 ** The mode is estimated from Fig. 2 for quartz-bearing or quartz-absent assemblages of WR I at 600 °C. There is no pyroxene or olivine in the reference assemblage.
 † Unpublished experimental results from recrystallization of olivine hornfels MP3-5 at 600 °C and 3 kbar in hydrothermal, cold-seal-bomb apparatus.

superscripts 0 and f indicate initial and final conditions. The mass-balance equations that show the distribution of the exchange components between phases in terms of the reaction vectors α, β, and γ and δ, ϵ, and ζ are in Table 8. Evaluation of the equations in Table 8 using the maximum and minimum limits of each exchange component yields equations for the exchange-component faces. The bounding-polygon planes are listed in Table 9. As one would expect, the planes of minimum exchange-component capacity are located around the origin (Figs. 9 and 10), and the planes of maximum exchange-component capacity are farthest from the origin. The plane [sh] limits amphibole composition to the range of all possible combinations of Tschermak, edenite, and plagioclase exchange and is the same as the shaded plane of Thompson et al. (1982) and Thompson (1982). For a more complete discussion of the derivation and construction of reaction

space, see Thompson et al. (1982), Thompson (1982), and Laird (1982a, 1982b).

The coordinates of the Morton Pass hornfels (Figs. 9 and 10 and Table 10) are found by multiple regression of the solutions of the four mass-balance equations derived from solving Equation 9 for TK, ED, PL, and MgCa$_{-1}$. The solution equations are in the form $A\alpha_n + B\beta_n + C\gamma_n = y_n$ and $A\delta_n + B\epsilon_n + C\zeta_n = y_n$. The coefficients A, B, and C of the independent variables are estimated by the method of constrained least-squares in which the dependent variable y is regressed on α, β, and γ and δ, ϵ, and ζ. To account for the differing magnitudes of the values of A, B, C, and y, the regression for each individual sample was weighted; however, weighting appears to have had only a small effect on the final result. No analysis errors were incorporated in this procedure, and therefore the errors are simply those of the regression. The correlation

TABLE 8. Mass-balance equations in terms of the exchange components for reaction polyhedra

Quartz tholeiite equations

TK: $(X^{f,tr} - X^{0,tr})n_{tr}^0 + (X^{f,di} - X^{0,di})n_{di}^0 = (X^{f,tr} - 0.875X^{f,di})\alpha + 0.125(6X^{f,di} - 1)\gamma$

ED: $(X^{f,tr} - X^{0,tr})n_{tr}^0 + (X^{f,di} - X^{0,di})n_{di}^0 = (X^{f,tr} - 0.875X^{f,di})\alpha - 0.125\beta + 0.75X^{f,di}\gamma$

PL: $(X^{f,tr} - X^{0,tr})n_{tr}^0 + (X^{f,ab} - X^{0,ab})n_{ab}^0 = (X^{f,di} - X^{0,di})n_{di}^0 = X^{f,tr}\alpha - X^{f,ab}\beta - (X^{f,ab} + 0.125)\gamma$

MgCa$_{-1}$: $(X^{f,tr} - X^{0,tr})n_{tr}^0 + (X^{f,di} - X^{0,di})n_{di}^0 = (0.063 + X^{f,tr} - 0.875X^{f,di})\alpha + 0.75X^{f,di}\gamma$

Olivine tholeiite equations

TK: $X^{f,tr} - X^{0,tr})n_{tr}^0 + (X^{f,di} - X^{0,di})n_{di}^0 = -X^{f,di}\delta + (X^{f,tr} - 0.5X^{f,di})\epsilon + (X^{f,di} - 0.167)\zeta$

ED: $X^{f,tr} - X^{0,tr})n_{tr}^0 + (X^{f,di} - X^{0,di})n_{di}^0 = (0.042 - X^{f,di})\delta - (0.026 - X^{f,tr})\epsilon + (X^{f,di} - 0.167)\zeta$

PL: $(X^{f,tr} - X^{0,tr})n_{tr}^0 + (X^{f,ab} - X^{0,ab})n_{ab}^0 + (X^{f,di} - X^{0,di})n_{di}^0 = 0.333X^{f,ab}\delta + (X^{f,tr} - 0.208X^{f,ab})\epsilon - (0.042 + X^{f,ab})\zeta$

MgCa$_{-1}$: $(X^{f,tr} - X^{0,tr})n_{tr}^0 + (X^{f,di} - X^{0,di})n_{di}^0 + (X^{f,fo} - X^{0,fo})n_{fo}^0 = (-X^{f,di} + 0.667X^{f,fo} + 0.167)\delta + (X^{f,tr} - 0.5X^{f,di} - 0.25X^{f,fo})\epsilon + X^{f,di}\zeta$
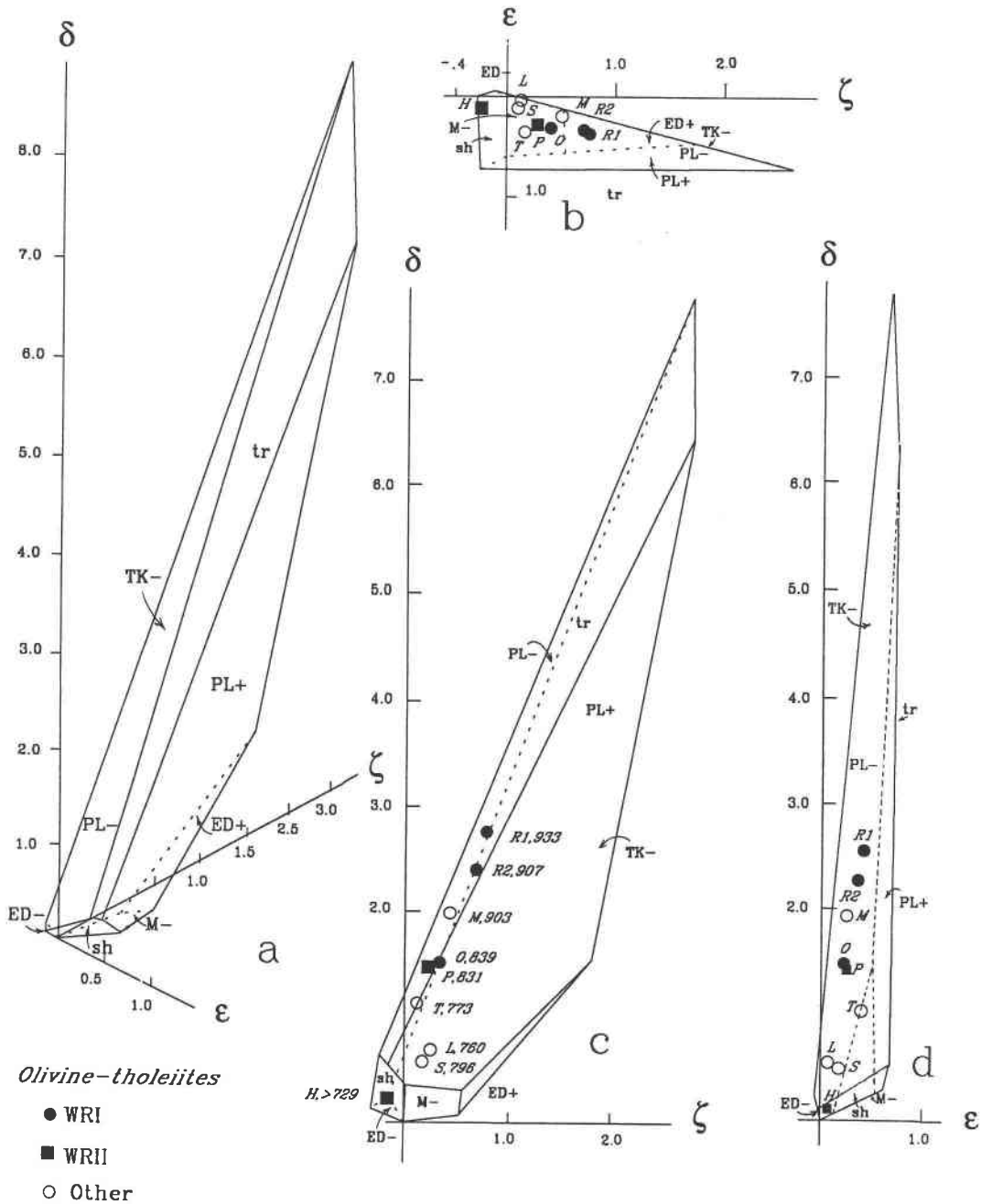
Fig. 10. (a) Oivine tholeiite reaction-space polygon corresponding to olivine hornfels MP3-5 of olivine tholeiite composition. The coordinate axes δ, ε, and ζ indicate to advancement along (net-transfer) Reactions 6, 7, and 8. The faces of the polygon are listed in Table 6 and are described in the caption to Fig. 9. MgCa₋₁ is abbreviated as M−. (b), (c), (d) are orthographic views. Letters refer to particular samples and correspond to the sample numbers and locations in Fig. 1 and temperatures in Table 4.

coefficients to the right in Table 10 indicate the percent to which the model describes each sample. In general, the model fits are excellent and suggest that other exchange components not utilized in the model are insignificant.

The location of an individual point in the reaction polyhedra is sensitive to the sample's bulk composition and very sensitive to the composition of the phases am-

phibole, plagioclase, and clinopyroxene. Hornfels in the quartz tholeiite space (Fig. 9) fall near the PL, ED, or TK faces. Many of these samples are layered and reflect a wide variety of compositions. It is interesting to note that WR I samples in the olivine tholeiite space (Fig. 10) fall on the same internal plane, indicating how close they truly are in composition. There also appears to be a sys-

TABLE 9. Equations for the bounding planes of polyhedra in Figs. 9 and 10

Equation	Plane
Quartz tholeiite	
$-0.655 = -\alpha$	[tr]
$-0.005 = 0.083\alpha + \beta - 0.25\gamma$	[qz]
$0 = 0.677\alpha - 0.125\gamma$	[TK−]
$0.867 = 1.125\alpha + 0.625\gamma$	[TK+]
$0 = 0.196\alpha + 0.125\beta + 0.75\gamma$	[ED−]
$0.527 = 0.125\alpha + 0.125\beta + 0.75\gamma$	[ED+]
$-0.169 = 0.137\alpha - \beta + 0.875\gamma$	[PL−]
$1.221 = 2\alpha - 0.502\beta + 0.377\gamma$	[PL+]
$0 = 0.258\alpha$	[MgCa$_{-1}$]
$0 = 0.063\alpha + 0.125\beta$	[sh]
Olivine tholeiite	
$0.658 = \epsilon$	[tr]
$0 = 0.667\epsilon + 0.167\zeta$	[TK−]
$0 = 0.042\delta + 0.17\epsilon + 0.042\zeta$	[ED−]
$0.529 = -0.958\delta + 0.474\epsilon + 1.042\zeta$	[ED+]
$-0.171 = -0.333\delta + 0.345\epsilon + 0.833\zeta$	[PL−]
$1.226 = -0.167\delta + 2.104\epsilon + 0.333\zeta$	[PL+]
$0 = -1.167\delta + 0.695\zeta$	[MgCa$_{-1}$]
$0 = 0.042\delta - 0.026\epsilon + 0.042\zeta$	[sh]

tematic increase in temperature as the trend of samples approaches the amphibole-out (tr) face in the olivine tholeiite model. This suggests that the progress of the whole-rock reactions for these rocks is dependent primarily upon temperature and not on other intensive variables. The systematic trend toward the amphibole-out face indicates that temperature-dependent reactions may also be the most important mechanism by which amphibole decreases modally in the assemblage.

DISCUSSION

It has been shown thus far that changes in amphibole composition in Morton Pass cannot be ascribed only to differences in bulk chemistry but are a function of the continuous and discontinuous reactions that occur during prograde metamorphism of the isochemical hornfels. Discontinuous reactions are chiefly responsible for changes in the modal abundance of phases and the development of facies and subfacies. Incremental net-transfer reactions where lowest-grade rocks are progressively transformed into their high-grade equivalents are a combination of continuous and discontinuous reactions.

The reaction-progress coordinates in terms of the net-transfer reactions α, β, γ and δ, ϵ, and ζ indicate the progress of each individual sample relative to the reference point. However, to estimate the progress of reactions of each incremental step between samples, the coordinates of the previous sample are subtracted out. Using WR I samples as examples allows specific progressive net-transfer reactions to be identified for each increase in metamorphic grade for a particular bulk composition.

The assemblage MP11-2A is the lowest-grade mafic schist at Morton Pass. The absence of chlorite and sodic

TABLE 10. Reaction progress values and model errors for Morton Pass quartz tholeiite and olivine tholeiite hornfels

Loc. in Fig. 1	Sample no.				Corr. coeff.*
		Quartz tholeiite			
		ξ_α	ξ_β	ξ_γ	
A2	MP11-2A	0.01 ± 0.01	0.26 ± 0.01	0.07 ± 0.01	1.00
F	83-10	0.03 ± 0.05	0.37 ± 0.03	0.16 ± 0.03	0.99
A1	MP11-1	0.05 ± 0.07	0.30 ± 0.03	0.11 ± 0.04	0.99
G	83-11	0.10 ± 0.00	0.29 ± 0.03	0.07 ± 0.00	1.00
I	83-12B	0.09 ± 0.03	0.21 ± 0.03	0.06 ± 0.03	0.96
E	MP18-1	0.13 ± 0.05	0.37 ± 0.05	0.14 ± 0.05	0.97
B	83-17A	0.07 ± 0.03	0.27 ± 0.03	0.08 ± 0.02	0.99
D	MP15-4	0.15 ± 0.01	0.31 ± 0.01	0.09 ± 0.01	1.00
N	MP6-4	0.18 ± 0.03	0.15 ± 0.04	-0.03 ± 0.04	0.96
Q	MP3-4	0.05 ± 0.02	0.34 ± 0.01	0.17 ± 0.01	1.00
		Olvine tholeiite			
		ξ_δ	ξ_ϵ	ξ_ζ	
H	83-19A	0.16 ± 0.40	0.07 ± 0.09	-0.24 ± 0.20	0.65
T	MP57-2	1.11 ± 0.14	0.37 ± 0.02	0.12 ± 0.07	0.99
S	MP57-9	0.56 ± 0.03	0.14 ± 0.00	0.09 ± 0.01	1.00
L	83-14	0.60 ± 0.04	0.05 ± 0.01	0.09 ± 0.02	1.00
P	83-16	1.48 ± 0.25	0.22 ± 0.03	0.25 ± 0.10	0.97
O	83-15	1.53 ± 0.22	0.30 ± 0.02	0.40 ± 0.10	0.98
M	83-18	2.03 ± 0.43	0.21 ± 0.04	0.25 ± 0.10	0.96
R2	MP3-6	2.34 ± 1.58	0.37 ± 0.10	0.68 ± 0.54	0.84
R1	MP3-5	2.63 ± 0.39	0.35 ± 0.03	0.70 ± 0.16	0.98
I	83-12B	1.19 ± 0.42	0.11 ± 0.07	0.23 ± 0.22	0.72
		Model results for data of Spear (1981)			
T2-80B (599 °C)		1.31 ± 0.73	0.20 ± 0.12	0.56 ± 0.28	0.65
T2-57A (651 °C)		2.21 ± 1.86	0.31 ± 0.18	1.08 ± 0.62	0.74
T2-81A (707 °C)		0.86 ± 0.60	0.23 ± 0.56	0.43 ± 0.24	0.95
T2-116A (802 °C)		0.86 ± 0.23	0.31 ± 0.00	0.15 ± 0.01	1.00
T2-102A (850 °C)		0.18 ± 0.81	0.29 ± 0.06	0.06 ± 0.35	0.95
T2-55A (655 °C)		-0.03 ± 0.04	0.13 ± 0.13	0.09 ± 0.03	0.99

* The planar correlation coefficients indicate the goodness-of-fit that solutions to Equations 14–17 and 18–21 (Table 9) have to a plane.

TABLE 11. Incremental net-transfer reactions for selected hornfels, indicating the reaction occurring from one hornfels to the next

T range	Reaction	(°C)
600 to ?	$0.019tr + 0.196ab + 0.066PL[amp,plg] + 0.066TK[amp] = 1.001qtz + 0.029MgCa_{-1}[amp] + 0.262ED[amp] + 0.019H_2O$	(10)
600 to 676	$0.048tr + 0.193ab + 0.105PL[amp,plg,pyx] + 0.105TK[amp,pyx] = 1.135qtz + 0.063di + 0.072MgCa_{-1}[amp,pyx] + 0.298ED[amp] + 0.048H_2O$	(11)
>676 to 729	$0.040tr + 0.101qz + 0.030ab + 0.057ED[amp] = 0.227di + 0.060MgCa_{-1}[amp,di] + 0.087PL[amp,ab,di] + 0.087K[amp,di] + 0.040H_2O$	(12)
>729 to 839	$0.760tr + 0.019ED[amp] + 0.684TK[amp,pyx] + 0.684PL[amp,plg,pyx] = 1.976di + 0.703ab + 1.14MgCa_{-1}[amp,pyx] + 0.76H_2O$	(13)
>839 to 907	$0.264tr + 0.249ab + 0.215ED[amp] = 0.456di + 0.132fo + 0.264MgCa_{-1}[amp,pyx] + 0.464PL[amp,plg,pyx] + 0.464TK[amp,pyx] + 0.264H_2O$	(14)

plagioclase indicates that MP11-2A is at a higher grade than the greenschist–hornblende hornfels transition. Epidote is not observed, possibly because the 3-kbar pressure is below its stability range (Liou et al., 1974; Apted and Liou, 1983). The modal abundance and composition of the phases in hornblende hornfels between the greenschist–hornblende hornfels transition and the first appearance of clinopyroxene are therefore affected by the reaction that transforms the reference-point hornfels into the lowest-grade rock MP11-2A (A2) by Reaction 10 (in Table 11). A certain amount of the continuous reaction

$$amp_1 + TK + ED + PL + MgCa_{-1} = amp_2 \quad (15)$$
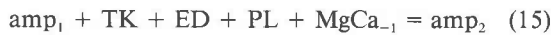
occurs at every stage of metamorphism. When combined with a fractional amount of Reaction 15 to represent the modal change of amphibole between the reference point amphibolite and sample MP11-2A, Reaction 10 becomes

$$0.159amp_1 + 0.196plg = 0.140amp_2 + 1.001qtz + 0.019H_2O. \quad (10a)$$
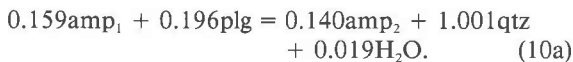
Clinopyroxene appears in the assemblage above 676 °C in quartz-bearing rocks by Reaction 11 (in Table 11). By adding in the continuous amphibole reaction and combining the exchange components with the additive components, the major reaction between the reference point and hornblende hornfels MP11-1 (WR I) becomes

$$0.203amp_1 + 0.193plg = 0.155amp_3 + 1.135qtz + 0.063di + 0.048H_2O. \quad (11a)$$
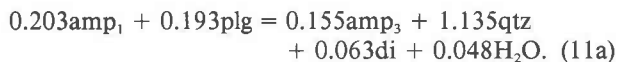
Although somewhat higher grade, hornblende hornfels 83-12B (WR I) does not differ greatly from MP11-1 in mineral chemistry or modal abundance; however, the modal decrease in quartz between the two (Fig. 2) suggests that quartz begins to react out. Reaction progress from MP11-1 to 83-12B gives the resultant Reaction 12 (in Table 11). Condensed into simplet form, the reaction is

$$0.646amp_3 + 0.101qtz + 0.030plg = 0.606amp_4 + 0.227cpx + 0.040H_2O. \quad (12a)$$
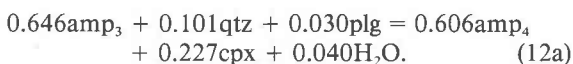
In the hornblende hornfels facies, Reaction 11a is the initial clinopyroxene-forming reaction operating in hornblende hornfels and appears to be initiated between >676

and >679 °C. Both Reactions 11a and 10a produce rather than consume quartz. The formation of quartz continues until amphibole becomes enriched enough in edenite component to react with quartz, as Reaction 12 suggests. Reaction 12a persists in the quartz-bearing hornblende hornfels from >679 °C until orthopyroxene begins to form. Although quartz generally is a common constituent of granulites, it continues to react out of the assemblage when orthopyroxene forms in the mafic schist. For example, in the orthopyroxene hornfels MP6-4 and MP3-4 (temperatures estimated at 827 and 889 °C), quartz is all but gone. Reaction 13 (in Table 11) is the resultant net-transfer reaction been hornblende hornfels 83-12B and orthopyroxene hornfels 83-15 (WR I) in olivine tholeiite space. When (1) the continuous amphibole reaction is added, (2) the pyroxene is expressed as clinopyroxene and orthopyroxene, and (3) Reaction 2 is combined to include quartz a representative reaction is derived:

$$1.48amp_{4a} + 4qtz = 0.720amp_{5a} + 1.465cpx + 0.511opx + 1.703plg + 0.76H_2O. \quad (13a)$$

This reaction expresses the mechanism by which quartz is removed from the assemblage. In quartz-poor hornfels, this reaction occurs over a small temperature interval. Stoddard (1985) observed similar reactions in the hornblende granulite facies terrane in the northwest Adirondacks, New York, but unfortunately did not indicate temperature ranges for his reactions. Quartz disappears from the assemblages of WR I before 840 °C. At this point, the major net-transfer reaction that operates in the orthopyroxene hornfels prior to the development of olivine (as exemplified by orthopyroxene hornfels 83-15) is

$$1.480amp_4 = 0.720amp_5 + 1.465cpx + 0.511opx + 0.703plg + 0.760H_2O. \quad (13b)$$
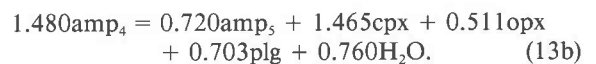
This reaction describes also the initial formation of orthopyroxene in SiO_2-undersaturated hornfels or the continued change in modal abundance.

The occurrence of olivine in high-grade mafic rocks is rare; however, the mechanism for its appearance is relatively straightforward. Olivine joins the assemblage at approximately 907 °C by Reaction 14 (in Table 11), which

transforms orthopyroxene hornfels 83-15 into olivine hornfels MP3-6 (WR I). The combined reaction is

$$0.677amp_5 + 0.249plg = 0.413amp_6 + 0.985cpx$$
$$+ 0.271opx + 0.132fo$$
$$+ 0.264H_2O. \quad (14a)$$
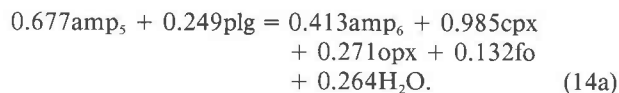
This reaction would continue until the ultimate demise of amphibole, predicted from Figure 2 to occur at about 1000 °C, when pargsite is the final reacting amphibole and no more amphibole can be formed. The continuous progressive decrease in modal amphibole shown in Figure 2 is consistent with Reactions 11a, 12a, 13a, and 14a above. Reactions 11a, 12a, and 13a show plagioclase on the reactants' side and Reaction 13a on the products' side, which is also consistent with the variation in the mode of plagioclase shown in Figure 2.

Ilmenite and magnetite are minor phases that play an important role in amphibole breakdown reactions. Generally they are found as products of amphibole dehydration in which ilmenite buffers the Ti content of the remaining amphibole. However, they are compositionally variable owing to low-temperature re-equilibration and do not show significant modal changes; hence, they have been ignored in the modeling.

It is not possible to predict an adequate reaction for the modal and compositional changes that occurred between the reference-point hornfels and the quartz-absent hornblende hornfels assemblage 83-19A (WR II). The olivine tholeiite model, which is strongly dependent upon the presence of pyroxene, gives a very poor model fit (Table 10). Coordinates for experimental runs by Spear (1981) under conditions analogous to metamorphism at Morton Pass, but where $P_{H_2O} = P_{TOT}$, are listed in Table 10. Even those experiments with excellent fits to the olivine tholeiite model do not lie in consistent placement with similar rocks at Morton Pass. Spear (1981) reported the first occurrence of clinopyroxene from reaction of hornblende and plagioclase at 768 ± 8 °C (1 kbar) and at 788 ± 8 °C (2 kbar) in olivine tholeiite experimental runs. The transition to granulite facies denoted by the first occurrence of orthopyroxene was experimentally determined by Spear (1981) at 794 ± 8 °C (1 kbar) and >805 °C (2 kbar) by reaction of hornblende with plagioclase for SiO_2-undersaturated rocks. In quartz-bearing rocks, orthopyroxene was determined to have formed at <745 °C (1 kbar) (Spear, 1981) and at 760 °C (1 kbar) and 780 °C (2.7 kbar) (Binns, 1968) by reaction of hornblende and quartz. Spear (1981) reported olivine to occur at 820 ± 15 °C (1 kbar) also by reaction of hornblende with plagioclase. These experimentally determined stability ranges of the subfacies, except for the olivine hornfels, are in agreement (within the large uncertainties for the calculated temperatures) with those at Morton Pass.

CONCLUSIONS

The primary effect of isochemical contact metamorphism of mafic schist in Morton Pass, Wyoming, was the change in abundance and composition of hornblende with concomitant changes in the proportion of other phases. Amphibole was progressively enriched in non-QUAD components as its modal abundance decreased and as QUAD component became unavailable, consequent to the formation of cpx, opx, and olivine. Because Al^{IV} has a systematic relationship with temperature, such non-QUAD enrichments with Al^{IV} are relevant to increases in temperature. Thus, it is suggested that the "evolution" of the non-QUAD components in amphibole can potentially give quantitative information on the intensive parameters of metamorphism. Progressive and systematic enrichment of F and Cl with decreasing amphibole abundance indicates that amphibole breakdown is purely a dehydration process and that both F and Cl may stabilize amphibole at high temperatures.

Reaction space provides an effective means for analysis of the progress of metamorphism in the mafic hornfels. Quartz-bearing mafic schist samples lie within the quartz tholeiite model, whose bounding planes are the limiting components of Reactions α, β, and γ. The sample coordinates lie somewhat scattered within the polygon with no apparent systematic relationship between them. The scattering indicates the effect that bulk composition has on the progress of any individual reaction. Comparatively, the nonlayered and therefore less compositionally variable samples of the olivine tholeiite compositions show that specific linear combinations of Reactions δ, ϵ, and ζ give resultant reactions that are strongly temperature dependent.

Analysis of reaction progress in quartz-bearing rocks indicates that quartz and clinopyroxene are products of the reaction between amphibole and plagioclase until >676 °C where quartz began to be consumed. Quartz completely disappeared by 900 °C; however, it was only a minor reaction constituent when orthopyroxene appeared between >679 and 825 °C. In mafic schist that had no quartz, reaction space involving olivine shows that clinopyroxene and orthopyroxene appeared in the assemblage between >729 and about 800 °C (e.g., WR II). The olivine hornfels subfacies denoted by the first occurrence of olivine formed at about 907 °C by the continued breakdown of amphibole. The culmination of metamorphism at Morton Pass was at 933 °C when amphibole was still a major constituent of the rock.

REFERENCES CITED

Abbott, R.N., Jr. (1982) A petrogenetic grid for medium and high grade metabasites. American Mineralogist, 67, 865–876.

Albee, A.L., and Ray, L. (1970) Correction factors for electron robe microanalysis of silicates, oxides, carbonates, phosphates, and sulfates. Analytical Chemistry, 42, 1408–1414.

Apted, M.J., and Liou, J.G. (1983) Phase relations among greenschist, epidote-amphibolite, and amphibolite in a basaltic system. American Journal of Science, 283-A, 328–354.

Bence, A.E., and Albee, A.L. (1968) Empirical correction factors for the electron microprobe analysis of silicates and oxides. Journal of Geology, 76, 382-403.

Binns, R.A. (1968) Hydrothermal investigations of the amphibolite-granulite–facies boundary. Geological Society of Australia Special Publication 2, 341–344.

Bochensky, P. (1982) Contact metamorphism effects of the Laramie Anorthosite Complex at Morton Pass, Wyoming. M.S. thesis, 55 p. University of Wyoming, Laramie, Wyoming.

Cameron, M., and Papike, J.J. (1979) Amphibole crystal chemistry. Fortschritte der Mineralogie, 57, 28–67.

Davidson, P.M., and Lindsley, D.H. (1985) Thermodynamic analysis of quadrilateral pyroxenes. Part II. Model calibration from experiments and applications to geothermometry. Contributions to Mineralogy and Petrology, 91, 390–404.

Engel, A.E.J., and Engel, C.G. (1962a) Progressive metamorphism of amphibolite interlayers, northwest Adirondacks, p. 37–82 Geological Society of America, Buddington Volume, New York (Boulder, Colorado).

———(1962b) Hornblendes formed during progressive metamorphism of amphibolites, northwest Adirondack Mountains, New York. Geological Society of America Bulletin, 73, 1499–1514.

Essene, E.J. (1982) Geologic thermometry and barometry. Mineralogical Society of America Reviews in Mineralogy, 10, 153–196.

Ferry, J.M. (1984) Phase composition as a measure of reaction progress and an experimental model for the high-temperature metamorphism of mafic igneous rocks. American Mineralogist, 69, 677–691.

Fowler, K.S. (1930) The anorthosite area of the Laramie Mountains, Wyoming. American Journal of Science, 5th ser., 19, Part I, 305–315 and Part II, 373–403.

Fuhrman, M.L. (1986) The petrology and mineral chemistry of the Sybille Monzosyenite and the role of ternary feldspars. Ph.D. dissertation, State University of New York at Stony Brook, Stony Brook, New York.

Fuhrman, M.L., Lindsley, D.H., Russ, C.A., and Frost, B.R. (1983) Contact relations between ferrosyenite and anorthosite of the Laramie Anorthosite Complex (LAC), Wyominig (abs.). EOS, 64, 327.

Fuhrman, M. L., Frost, B.R., and Lindsley, D.H. (1988) Crystallization conditions of the Sybille monzosyenite, Laramie Anorthosite Complex, Wyoming. Journal of Petrology, 29, 699–729.

Graff, P.J., Sears, J.W., Holden, G.S., and Hausel, W.D. (1982) Geology of the Elmers Rock greenstone belt, Laramie Range, Wyoming. Geological Survey of Wyoming, Report No. 14, 23 p.

Hammerstrom, J.M., and Zen, E. (1986) Aluminum in hornblende: An empirical igneous geobarometer. American Mineralogist, 71, 1297–1313.

Harte, B., and Graham, C.M. (1975) The graphical analysis of greenschist to amphibolite facies mineral assemblages in metabasites. Journal of Petrology, 16, 347–370.

Hynes, A. (1982) A comparison of amphiboles from medium- and low-pressure metabasites. Contributions to Mineralogy and Petrology, 81, 119–125.

Klugman, M.A. (1966) Resume of the geology of the Laramie Anorthosite Mass. Mountain Geologist, 3, 75–84.

Laird, J. (1980) Phase equilibria in mafic schist from Vermont. Journal of Petrology, 21, 1–37.

———(1982a) Amphiboles in metamorphosed basaltic rocks: Greenschist facies to amphibolite facies. Mineralogical Society of America Reviews in Mineralogy, 9B, 113–137.

———(1982b) Amphiboles in metamorphosed basaltic rocks: Blueschist-greenschist-eclogite relations. Mineralogical Society of America Reviews in Mineralogy, 9B, 138–159.

Laird, J., and Albee, A.L. (1981a) High pressure metamorphism of mafic schist from northern Vermont. American Journal of Science, 281, 97–126.

———(1981b) Pressure, temperature, and time indicators in mafic schist: Their application to reconstructing the polymetamorphic history of Vermont. American Journal of Science, 281, 127–175.

Leake, B.E. (1965) The relationship between composition of calciferous amphibole and grade of metamorphism In W.S. Pitcher and G.W. Flynn, Eds., Controls of metamorphism, p. 299–318. Wiley, New York.

Lindsley, D.H. (1983) Pyroxene thermometry. American Mineralogist, 68, 477–493.

Lindsley, D.H., and Andersen, D.J. (1983) A two-pyroxene thermometer. Proceedings of the 13th Lunar and Planetary Science Conference, Journal of Geophysical Research, 88, Supplement, A887–A906.

Liou, J. G., Kuniyoshi, S., and Ito, K. (1974) Experimental studies of the phase relations between greenschist and amphibolite in a basaltic system. American Journal of Science, 274, 613–632.

Nabelek, C. R., and Lindsley, D.H. (1985) Tetrahedral Al in amphibole: A potential thermometer for some mafic rocks. Geological Society of America Abstracts with Programs, 17, 673.

Newhouse, W.H., and Hagner, A.F. (1957) Geological map of anorthosite areas, southeastern part of Laramie Range, Wyoming. U.S. Geological Survey Mineral Investigations Field Studies, Map MF 119.

Papike, J.J., Cameron, K.L., and Baldwin, K. (1974) Amphiboles and pyroxenes: Characterization of other than quadrilateral components and estimates of ferric Fe from microprobe data. Geological Society of America Abstracts with Programs, 6, 1053.

Robinson, Peter. (1982a) Metamorphosed igneous rocks at high temperature: The breakdown of amphiboles. Mineralogical Society of America Reviews in Mineralogy, 9B, 182–206.

———(1982b) Amphiboles in metamorphosed calcareous sedimentary rocks. Mineralogical Society of America Reviews in Mineralogy, 9B, 206–207.

Russ, C.A. (1984) Contact metamorphism of mafic schist, Laramie Anorthosite Complex, Morton Pass, Wyoming. M.S. thesis, 111 p. State University of New York at Stony Brook, Stony Brook, New York.

Russ, C.A., and Lindsley, D.H. (1984) Prograde contact metamorphism of mafic schist, Morton Pass, Laramie Mtns., Wyoming. EOS, 65, 291

Spear, F.S. (1981) An experimental study of hornblende stability and compositional variability in amphibolite. American Journal of Science, 281, 697–734.

Spencer, K.J., and Lindsley, D.H. (1981) A solution model for coexisting iron-titanium oxides. American Mineralogist, 66, 1189–1201.

Stoddard, E.F. (1985) Zoned plagioclase and the breakdown of hornblende in pyroxene amphibolites. Canadian Mineralogist, 23, 195–204.

Stormer, J.C. (1975) A practical two-feldspar geothermometer. American Mineralogist, 60, 667–674.

Thompson, A.B. (1976) Mineral reactions in pelitic rocks: I. Prediction of P-T-X (Fe-Mg) phase relations. American Journal of Science, 276, 401–424.

Thompson, J.B., Jr. (1982) Reaction space: an algebraic and geometric approach. Mineralogical Society of America Reviews in Mineralogy, 10, 33–52.

Thompson, J.B., Jr., Laird, J., and Thompson, A.B. (1982) Reactions in amphibolite, greenschist and blueschist. Journal of Petrology, 23, 1–27.

van der Plas, L., and Tobi, A.C. (1965) A chart for judging the reliability of point counting results. American Journal of Science, 263, 87–90.